Eng. Sci., 2020, 11, 54-65

Engineered Science

DOI: https://dx.doi.org/10.30919/es8d1118

Higher Voltage Redox Flow Batteries with Hybrid Acid and Base Electrolytes

Mohsen Torabi Dizaji[1] and Wenzhen Li[1,2,*]

Abstract

An organic redox flow battery with hybrid acid and base electrolytes using a single cation exchange membrane has been successfully developed to demonstrate higher operation voltage and higher energy density. This concept of hybrid electrolyte flow battery was able to increase the voltage span of a previously tested quinone flow battery by 300 mV and raise the energy density by four times to reach 27.4 Wh/L. This technique has been successfully implemented in another flow battery system utilizing metal ions, demonstrating the applicability of this technique to other types of redox flow batteries. Furthermore, the suggested flow batteries with hybrid electrolytes have been proposed to be economically advantageous over the systems using a cation-exchange membrane and an anion-exchange membrane simultaneously.

Keywords: Redox flow batteries; Hybrid electrolytes; Energy storage; Membranes; Quinone redox mediators.
Received: 9 May 2020; Accepted: 27 July 2020.
Article type: Research article.

1. Introduction

Intermittency is one of the main barriers in the route of widespread harvesting of the immense amount of renewable energy, such as wind and solar, that is provided freely by mother nature.[1-3]While technologies, such as pumped hydroelectric[4] and compressed air energy storage[5] might be feasible for a very large scale, imminent decentralization[6] of power grids will highlight the needs of efficient small-scale energy storage systems such as batteries.[7,8] Traditional batteries have provided a feasible means to renewable energy storage,[9] however, they suffer from various hurdles, such as dendrite formation in solid-state metal-based batteries[10,11] or mechanical electrode damage in intercalation battery systems.[12,13] In contrast, redox flow batteries possess valuable capabilities, such as the ability to use redox components with lower cost, easier scale-up, and decoupling of the energy and power sections. The energy capacity of a flow battery will increase by enlarging the size of the storage tanks and the output power can be manipulated via modification of the battery cell.[14]

Metal ion-based flow batteries, such as all-vanadium, iron-chromium and zinc-bromine flow batteries are commercially available, however, they face great challenges such as high material cost,[15] slow kinetics,[16-18] precipitation[19] and corrosion[20,21] (for all-vanadium flow batteries), side reactions,[17] efficiency[17] and corrosion (for iron-chromium flow batteries), dendrite formation,[22] environmental hazards related to maintaining all components in solution phase[23] and requirements for cooling[24] (for zinc-bromine flow batteries). In comparison, organic flow batteries can serve as a reliable alternative for lowering material costs and improving kinetics.[25] In general, organic compounds have higher tunability, and it is possible to modify their redox potential, solubility as well as other attributes through proper functionalization.[26] Sensitivity analysis of the capital cost of the vanadium flow batteries has highlighted the importance of electrolyte costs,[15] a conclusion that is applicable to other flow batteries as well. Exploring cheaper components as substitutes for vanadium-based redox mediators can reduce the total cost of energy storage,[27] and organic compounds with lower cost and good redox characteristics can provide advantages over other types of redox flow batteries.[28] In addition, aqueous organic flow batteries are able to operate at higher current densities.[29-33]

Currently, organic redox flow batteries suffer severely from low energy density. Quinones, by providing two

[1] *Department of Chemical and Biological Engineering, Iowa State University, 618 Bissell Road, Ames, Iowa 50011, United States.*
[2] *US Department of Energy Ames Laboratory, 2408 Pammel Drive, Ames, Iowa 50011, United States.*
**E-mail: wzli@iastate.edu (W. Li).*

© Engineered Science Publisher LLC 2020

electrons in their redox reactions, exhibiting high kinetic rates and remarkable solubility, appears to be one of the promising candidates for organic redox flow batteries.[32,34-36] These commendable properties make them good candidates for energy storage systems with high power requirements.[37] Via modifications with proper functionalities, water solubility of the quinone compounds can be increased.[38,39] Furthermore, they can be used both as catholyte and anolyte in the aqueous flow batteries.[40] The redox potentials of quinone compound heavily depend on the electrolyte pH. Thus, unfortunately, upon increasing the system pH, the redox potential of the anode will become more negative with 59 mV/pH, but the redox potential of the cathode will become less positive with 59 mV/pH. Similarly, by reducing the pH, the opposite shift will occur. Therefore, any fixed pH electrolyte will just bring a potential gain from one side and a potential sacrifice from the other side, and no net benefit can be gained. Thus, benefiting from the entire potential range of the quinones at a specific pH becomes infeasible, leading to a lower operation voltage and thus lower energy density. Consequently, quinone compounds need to be coupled to other redox mediators (e.g. $[Fe(CN)_6]^{-4}$) to achieve higher operation voltages at a specific pH.

In an elegant work done by Yan group,[41] two ion-exchange membranes were used in flow batteries. Their system included one anion exchange membrane (AEM) and one cation exchange membrane (CEM) with an electrolyte between the two membranes. This hybrid membrane battery has successfully coupled various redox groups together to reach higher voltages. However, the two membrane batteries will inevitably add extra costs, and this becomes more pronounced for a large flow battery system that benefits from a large amount of ion-exchange membranes, thus imposing more fixed capital costs to the battery system.

Herein, we introduced a methodology, that directly utilizes anolyte and catholyte with contrasting pH on two sides of a cation exchange membrane, enabling a high voltage flow battery. This scheme permits maximizing the redox potential difference between the cathode and the anode via adjusting their pH separately. Cathodic quinone has a more positive redox potential at a lower pH, while the anodic quinone has a more negative redox at a higher pH. Thus, both the overall voltage and the energy density of the hybrid-pH electrolyte battery will significantly increase. In detail, 1, 2-hydroquinone-3, 5-disulfonic acid (HQDS) and 2, 6-dihydroxy anthraquinone (DHAQ) are employed as the cathode and the anode mediators, respectively, with redox reactions shown below (Eqs. (1) and (2)):

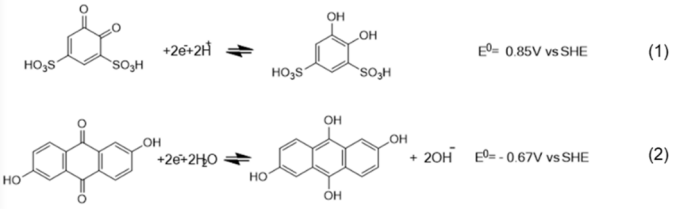

When coupled to anthraquinone sulfonic acid in an acidic environment, 1,2-Hydroquinone-3,5-disulfonic acid (HQDS) has displayed a high redox potential (+0.85 V).[40,42] Hydroquinone disulfunic acid is very safe in comparison to the hazardous bromine and displays advantages over ferricyanide ion. First, due to the presence of two sulfonic acid groups in HQDS, it has a high solubility (>1.7 M) in aqueous systems even in neutral pH. Second, it entails two electron transfers per its redox reaction and also, its redox potential can be as high as 0.86 V in acidic solutions. In contrast to ferricyanide ion which its solubility is limited to 0.4 M in alkaline media and is not stable in acidic media, incorporates just one electron in its reaction and its redox potential is independent of pH thus, rendering the potential benefits accrued by pH reduction infeasible and moreover, ferricyanide ion has been proven to be unstable during electrochemical reactions in alkaline environments.[43] Utilization of HQDS as catholyte significantly increases the energy density of the system due to its higher concentration and entailing two electrons per redox reaction.

2, 6-dihydroxyanthraquinone (DHAQ) has shown to serve as a reliable anode mediator for alkaline quinone flow batteries with a good redox potential of -0.67 V (vs SHE) and displaying good reversibility (fast kinetics) when it was coupled to potassium ferricyanide,[44] and it can also show good durability.[45] The redox potential of DHAQ will become more negative by raising the solution pH (till 12), however, reaching concentrations as high as 0.55 M, necessitates using solutions with higher alkalinity (2 M KOH), which also provides sufficient capacity for the alkalinity of the system, preventing the necessity for a buffer solution at the anode side. Overall, this hybrid battery can provide an equilibrium potential of 1.5 V and an energy density of 27.41 Wh/kg.

It is worth mentioning that successful uses of hybrid electrolytes for lithium ion batteries have enabled the energy storage system to reach higher operating voltages. For example, an ionic liquid at the cathode and a super concentrated ether based electrolyte at the anode, are separated by one layer of Nafion membrane with intercalated electrodes and can reach a high voltage of 4.2 V.[46] Similarly, coupling Li/Pyr_{13}TFSI to equimolar LiTFSI/G3 complex and utilizing $LiNi_{0.5}Mn_{1.5}O_4$/graphite cathode can deliver an operating voltage of 4.7 V, with an excellent capacity retention.[47]

This research has demonstrated that in principle all quinone flow batteries can be modified to accommodate an alkaline solution in the anode side and an acidic solution in the cathode side, using a single cation-exchange membrane to maximize the benefit gained from pH-dependent redox potential of the quinone compounds that rely on deprotonation. Using a high capacity buffer solution with pH=0.3 on the cathode side as well as electrolyte makeup injection (e.g. via a HPLC pump) will prevent potential drop of the battery and similarly addition of KOH to anode electrolyte will ensure sustaining high pH levels in the anode and prevent precipitation of DHAQ.

© Engineered Science Publisher LLC 2020

2. Experimental

2.1 Materials

All materials were used as received. Anthraflavic acid (2,6-dihydroxy anthraquinone) 90% and Potassium Hydroxide 85% were purchased from Sigma. Dibasic potassium phosphate 99.4%, Potassium Chloride 100% and Hydrochloric Acid 36.9% were purchased from Fisher Scientific. 1,2-Dihydroxybenzene-3,5-disulfonic acid disodium salt monohydrate 97% was purchased from Alfa Aesar. Nafion 212, Carbon paper (Sigracet 39 AA) as well as Single cell hardware including end plates, collectors, POCO graphite flow channel plates were purchased from fuel cell technologies.

2.2 Cyclic Voltammetry

All half-cell tests were purged by argon during operation to prevent any oxidation with air. A three-electrode cell was used to carry out cyclic voltammetry. Platinum wire and Ag/AgCl in 3 M KCl (0.210 V vs. SHE) were used as the counter and reference electrodes respectively. Working electrode was glassy carbon electrode with diameter of 5 mm. Scan rate was 100 mV/s in all CV tests except the Randles-Sevcik test that the scan rates were 25, 50, 75, 100, 125, 150, 175, 200, 250, 300, 350, 400, 450, 500 mV/s. 2 mM DHAQ in 1 M KOH was tested from -1.1 V to -0.1V vs Ag/AgCl and 2mM of HQDS in a solution made of 0.5 M KCl and 1 M HCl with PH=0.3 was tested from 0 V to 1.2 V vs Ag/AgCl. Different mixtures of (0.2 M) Potassium Phosphate Dibasic (K_2HPO_4) and (1 M) Hydrochloric Acid were used to prepare a series of buffer solutions with pH ranging from 1-7 to run cyclic voltammograms with 5 mM HQDS to prepare the pourbaix diagram. Pourbaix, RDE tests were only performed for the cathode active material (HQDS) because similar tests for DHAQ were performed and reported by Aziz *et al* (2015).

2.3 Rotating Disc Electrode

Rotating disc electrode tests were performed using a Pine MSR rotator instrument using a similar setup as the one used in cyclic voltammetry. The following rotation speeds were used in this test: 300, 400, 600, 800, 900, 1000, 1200, 1400, 1600, 1800, 2000, 2200 and 2400 RPM. RDE tests were performed for two cases. 2 mM HQDS dissolved in a solution with pH=0.3 made of KCl (0.5 M) & HCl (1 M) and also for the solution alone to measure the background currents for subtraction from the main measured currents.

2.4 Galvanostatic charge/discharge

The cell was assembled according to the improved no-gap structure.[48] The cell design was in a manner to minimize dead zones and optimize flow distribution.[49] Pretreatment of Nafion212 (&211) was performed first by boiling it in DI water at 85°C for 35minutes, then treating with 5% H_2O_2 solution at 85°C and soaking it overnight at 0.1 M KOH. POCO graphite serpentine flow channel plates sandwiched between gold plated copper current collectors were used on both sides. Carbon paper (Sigracet 39AA) was baked in an oven at 400°C for 24 hrs and three layers of 39 AA, compressed to 80% of the initial thickness with an area of 4cm^2 were used on both sides of the membrane. Compression and sealing are guaranteed by the number and thickness of PTFE gaskets used between current collectors and flow channel plates. All tests were performed using a Biologic VSP-300 potentiostat. The flow rate was controlled to be 100 ml/min using Cole-Palmer Masterflex pumps. Further increase in the flow rate didn't show a noticeable decrease in the mass transfer resistance of the system.[37] The batteries were charged to 2 V during charging and 0.3 V during discharging (0.5 V for the case of HQDS with N211). Cathode pH is sustained via intermittent injection of 0.6 ml/hr of 1 M HCl by the aid of a ChromTech hplc pump equipped with PEEK head that is tolerant against this concentration of hydrochloric acid. 20% of isopropanol in DI water was used as the flushing liquid. The pH of the anode is maintained by intermittent checking and modifying the pH via adding KOH to anode tank. Both tanks were purged by argon gas throughout the experiment to avoid any reactions with oxygen. Efficiencies were calculated according to the following equations (Eqs. (3-5)):[26]

$$E=\eta_C=\frac{Q_D}{Q_C} \tag{3}$$

$$VE=\eta_V=\frac{\int_0^{T_D} E_D(t)dt/T_D}{\int_0^{T_C} E_C(t)dt/T_C} \tag{4}$$

$$EE=\eta_{EE}=\eta_C.\eta_V \tag{5}$$

where *CE*, *VE* and *EE* are columbic, voltaic and energy efficiency respectively. C, D and *T(t)* stand for charging, discharging and time respectively. η is efficiency.

3. Results and Discussion

3.1 Cyclic Voltammetry

Cyclic voltammetry is conducted to compare the redox potential and the reversibility of both quinone compounds to be used in the flow battery. The pH of the anolyte and catholyte is maintained at 14, 0.3, respectively, to obtain maximum benefit from pH. The redox potentials of vf DHAQ (in anolyte) and HQDS (in catholyte) are at -0.67 V and 0.85 V, respectively, as shown in Fig. 1. Both two redox mediators display distinguishable redox potentials and good reversibility, while the reversibility of DHAQ is higher than the reversibility of HQDS, which indicates faster redox kinetics of DHAQ than HQDS, this surely can be attributed to its chemical structure, but also partly related to the alkaline reaction media for DHAQ, that doesn't need the protonation steps between redox reactions, which slow down the electrochemical kinetics in an acidic media.[50]

 © Engineered Science Publisher LLC 2020

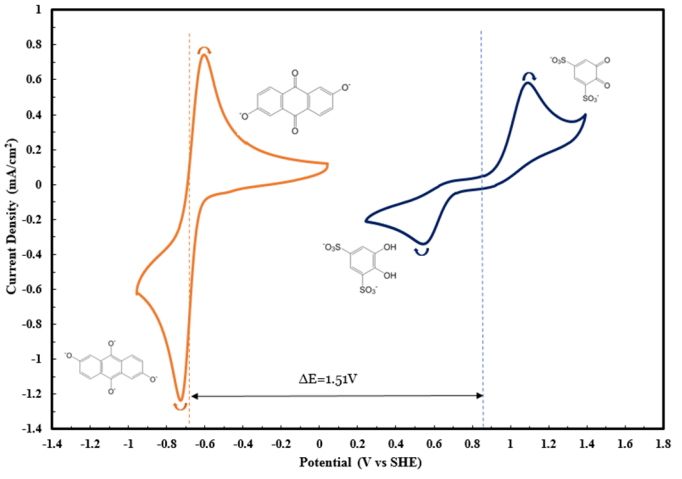

Fig. 1 Cyclic voltammogram (CV) of 2 mM DHAQ in 1 M KOH (orange curve) and 2 mM HQDS in buffer solution pH=0.3 (with 0.5 M KCl and 1 M HCl) (dark blue curve) scanned at 100 mV/s on glassy carbon electrode. Direction of scans is exhibited by arrows. Dashed lines represent the redox potentials. Oxidized and reduced chemicals forms are illustrated on the CVs. Test was done at room temperature(25 °C).

3.2 Electrochemical stability

Cyclic Voltammograms at various scan rates are carried out to test the stability of the cathode active material (hydroquinone disulfunic acid, HQDS) as well as its compatibility with the components of the buffer solution within the potential range of the battery operation. Randles-Sevcik test is performed with 2 mM of HQDS in a 0.5 M KCl buffer solution with pH=0.3 made with 1 M HCl. Cyclic Voltammograms are performed from 0 V to 1.1 V vs Ag/AgCl with scan rates ranging from 20 mV/s to 500 mV/s as shown in Fig. 2, yielding a linear plot of peak current densities (oxidation) vs square root of scan rates, providing a proof for the stability of the catholyte. Cycle #6 is considered as the basis of the calculations.

3.3 Pourbaix analysis

Pourbaix analysis is provided to estimate the voltage benefit gained by reducing the pH of catholyte and using the hybrid battery system. Theoretically, it is expected to have gained by lowering the pH of the system due to the participation of protons in the redox reactions, however, this might not be true for some kind of Quinone compounds,[44] thus a Pourbaix analysis is helpful. Pourbaix Diagram is performed by running CVs of 5 mM HQDS in buffer solutions of various pH made up of varying proportions of K_2HPO_4 (0.2 M) and HCl (1 M). Scanning is performed with a rate of 100 mV/s from 0 V to 1.2 V vs Ag/AgCl as shown in Fig. 3. Cycle #6 is considered as the basis of calculation.

The analysis results clearly illustrate the gains in the redox potential of the system by reducing system pH, thus highlighting the benefit of using electrolytes with contrasting pH on both sides of the cation-exchange membrane. Furthermore, a reduction in catholyte reversibility is observed upon increasing the pH from 1 to 2, which provides us with another benefit accrued by keeping the pH of catholyte as low as 0.3. By comparing the reversibility, it is noticed that the decrease in reversibility is less severe when pH is increased from 2 to 7. This sudden reduction in reversibility upon changing pH from 1 to 2 may impose higher kinetic overpotential in a single cell test, and it can be attributed to the mechanism change of redox reaction. At high proton concentrations (e.g. pH<1), the redox reaction initiates with the protonation step; while at lower proton concentrations (higher pH values), the onset reaction is the electron transfer, which is the rate-limiting step in this case.[50] This change of paradigm seems to occur at around pH=2 for HQDS based on this observation. Furthermore, a significant reduction in proton concentration might also negatively affect the rate of the second proton transfer, which reduces the overall reaction rate. Injection of cathode redox mediators can successfully prevent this issue.

Pourbaix analysis of the DHAQ that is performed by Aziz group (2015) has demonstrated that the redox potential is reduced with the increase of the pH to 12, and after that the redox potential remains constant at -0.67 V. However, reaching a concentration of 0.55 M DHAQ need its dissolution in 2 M KOH [44]. Thus, it is necessary to maintain the anode at pH=14 and the cathode at pH=0.3.

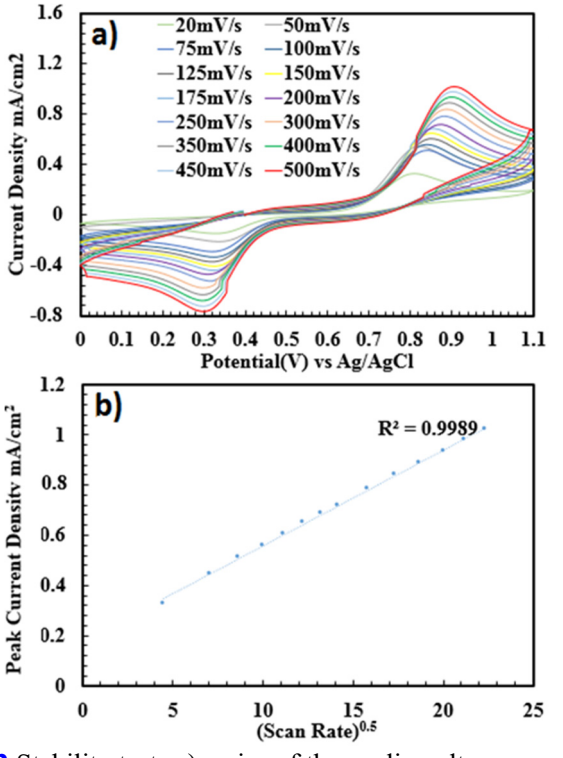

Fig. 2 Stability tests a) series of the cyclic voltammograms of HQDS taken at different scan rates, b) peak current densities vs square root of scan rate. Electrolyte pH=0.3 and the test was run at room temperature (25 °C).

© Engineered Science Publisher LLC 2020

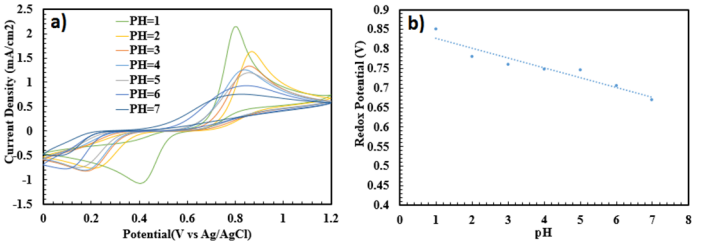

Fig. 3 Pourbaix Analysis a) series of cyclic voltammograms for 5mM HQDS at different pHs. b) Pourbaix diagram plotted based on the results of the graph a.

3.4 Rotating Disc Electrode Analysis

Rotating disc electrode (RDE) tests can provide kinetic information of the redox mediators used in the batteries by calculating the exchange current density, reaction constant and identifying the kinetically limiting component. RDE is performed with 2 mM of HQDS dissolved in a buffer solution of pH=0.3 (0.5 M KCl & 1 M HCl). Potential is scanned from 0 V to 1.1 V vs. Ag/AgCl reference electrode. Oxygen evolution reaction (OER) becomes appreciable when the potential approaches 1.2V in an acidic environment, this requires a reduction of the background currents from the derived results prior to making L-K calculations. Potential scanning is done at the rate of 100 mV/s by varying the rotation speeds from 300 RPM to 2800 RPM with and without the cathode mediators, and the results are collected after subtraction of the background currents (shown in Fig. 4), thereafter, via L-K & Tafel calculations, the exchange current density, as well as reaction rate constant are extracted as shown in Fig. 4b, c & d.

The slope of the Levich plot was calculated to be 0.012 mA/(Rad $^{0.5}$ s $^{0.5}$) by considering the kinematic viscosity as 1.08×10^{-6} m^2/s, the diffusivity coefficient was calculated to be 2.9×10^{-6} cm^2/s, which was close to the reported value in the acidic environment.[42] L-K plots were derived by plotting the inverse of the current vs the inverse of the square root of the rotation speed at various overpotentials. The Y-intercept of these plots gives the inverse of the kinetic current that was used in logarithmic scale vs overpotentials to give the Tafel plot. Exchange current density and the reaction rate constant were calculated to be 6.3×10^{-5} A/cm^2 and 1.63×10^{-4} cm/s respectively. Rate constant of HQDS redox reaction is lower than that of the DHAQ redox reaction published in the literature (7×10^{-3} cm/s), which makes the cathode mediator a kinetically limiting component.

3.5 Battery Performance

Galvanostatic cycling tests are performed at ambient condition (25 °C) with 8 ml of 0.55 M DHAQ dissolved in 2 M KOH and 5 ml of 0.9 M HQDS and 0.5 M KCl dissolved in a solution with pH=0.3 (made with 1 M HCl) at various charging/discharging currents. The cell consisted of gold covered copper plates, serpentine graphite flow channel plates, treated carbon paper as well as Nafion (211&212) membrane.

Cycling test with Nafion 211, displays the highest voltage efficiency as well as an open circuit voltage of 1.5 V, when charging/discharging with a current of 300 mA. Cycling tests are repeated with Nafion N212, exhibiting a higher coulombic efficiency perhaps due to lower crossover resulted from the higher thickness of the cation-exchange membrane. Long term test is performed with 8 ml of 0.55 M DHAQ dissolved in 2 M KOH for anolyte and 8 ml of 0.9 M HQDS and 0.5 M KCl dissolved in a solution with pH=0.3 for catholyte. Therefore, the kinetically limiting part (cathode) was sustained at a stoichiometrically excess condition. Due to deactivation of HQDS, this material is added during intervals to the catholyte to prevent deterioration of the battery performance. 1 M HCl is added intermittently to the catholyte via a hplc pump, while solid KOH is added intermittently to the anolyte. The flow battery is charged with a current density of 80 mA/cm^2 and discharged with a current density of 40 mA/cm2 in the range of 0.3 V to 2.0 V, reaching a coulombic efficiency of 99%. Cycling was continued for more than 140 hours with system pH measurements during intervals, demonstrating that the final catholyte pH (0.3) was similar to its initial pH of 0.3, displaying a successful manifestation of the long-term operation of a flow battery utilizing electrolytes with contrasting pH on both sides of a cation-exchange membrane. Two typical cycles are presented in Fig. 5. Furthermore, polarization curves of the flow battery are prepared via linear sweep voltammograms (LSV) performed at a scan rate of 100 mV/s at three increments of 10%, 50% and 100% of the state of charge. The flow battery is able to reach a peak power density of 286 mW/cm2 at room temperature, suggesting its promise of practical operation.

In this flow battery, anolyte and catholyte contain KOH and KCl, respectively. This configuration ensures the presence of sufficient amount of K^+ at both sides of the CEM, which has also been saturated with K^+ by soaking in 0.1 M KOH solution overnight before use. Potassium ion (K^+) is the main charge carrier to be transferred through the cation-exchange membrane under the charging and discharging cycles of the battery.

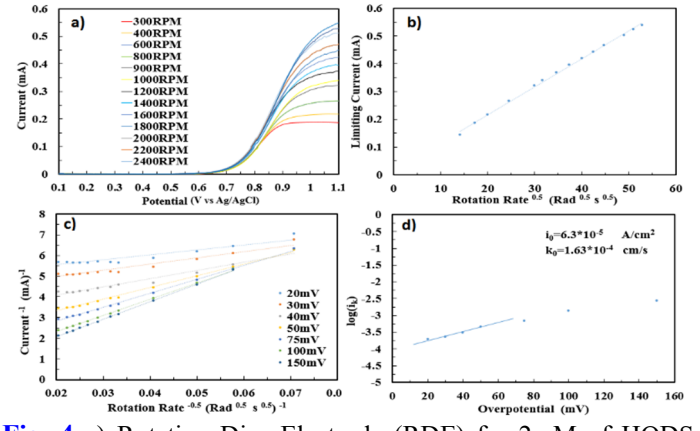

Fig. 4 a) Rotating Disc Electrode (RDE) for 2mM of HQDS dissolved in a buffer solution with pH=0.3 b) Levich plot, c) Levich-Koutecky plot & d) Tafel plot.

© Engineered Science Publisher LLC 2020

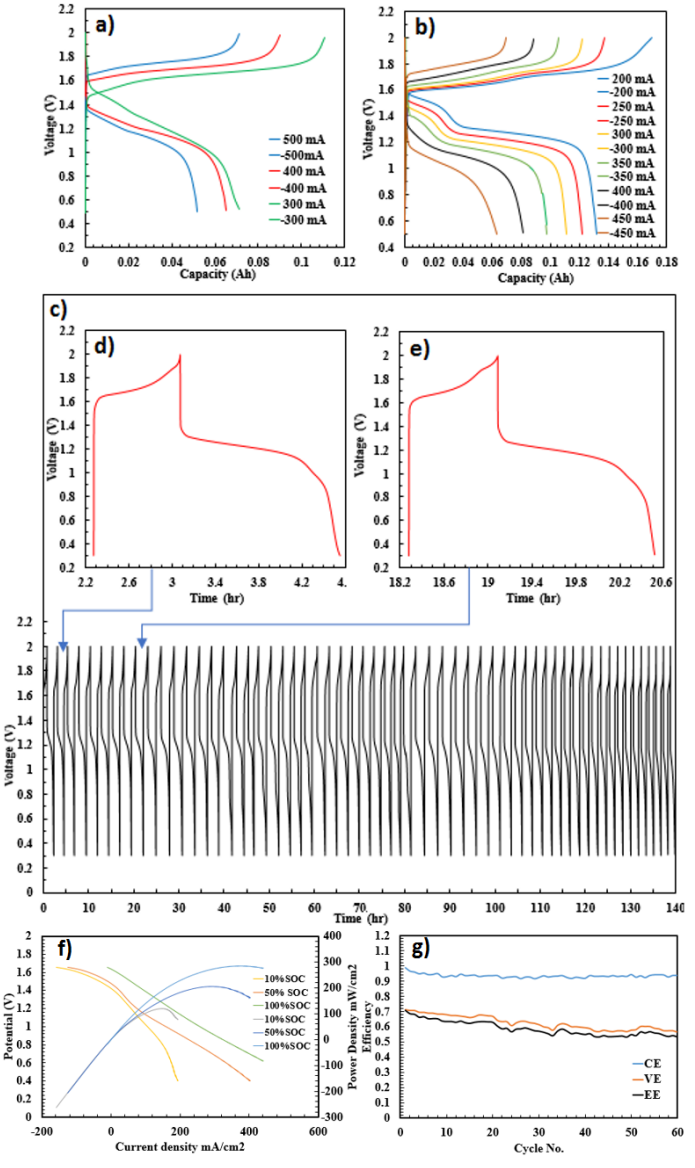

Fig. 5 Performance of the DHAQ vs HQDS flow battery with hybrid acid and base electrolytes a) Galvanostatic cycling with Nafion 211, b) Galvanostatic cycling with Nafion 212, c) Durability test for the system with N212, charging current 80mA/cm^2 and discharging current 40 mA/cm^2 d & e) two selected sample cycles, f) polarization curve with 10%, 50% and 100 % state of charge, g) battery efficiency during 60 cycles.

In addition, in a separate test, when acid injection to the catholyte is stopped, frequent pH measurement of both the cathode and anode tanks by a portable pH meter shows a reduction of the anolyte pH as well as an increase of the catholyte pH, which indicates that protons were also carried through the CEM. In the main cycling test that KOH and 1 M HCl were added intermittently to the anolyte and catholyte and the pH was measured at intervals, pH remained constant after 140 hours of operation.

3.6 Electrochemical Impedance Spectroscopy

Dissecting the resistance of a flow battery can help to identify high impedance areas inside the battery and seek for proper mitigation strategies. High frequency resistance (ohmic) is mainly due to ionic movement inside the membrane as well as ionic, electric and contact resistances in electrodes and electric resistance through the 3D porous structure of electrodes. On the other hand, low frequency impedance allows calculation of the kinetic loss. The flow battery is charged with 1C-rate incrementally (10%) from zero charges to full charge. 100% charging of the system was attained through keeping battery operating at 2 V until the current fell below 50 mA. In each increment, electrical impedance spectroscopy (EIS) is performed in the range of 200 kHz to 20 Hz, and the high frequency resistance is measured as the x-intercept of the graph and the polarization resistance is estimated by extrapolation of the Nyquist semicircles to the x-axis. Both ASRs (high frequency, polarization) were plotted against SOC% as shown in Fig. 6a. Ohmic resistance of the battery remain almost constant at different states of charge and the flow battery shows a kinetic polarization which can be attributed to the catholyte as shown in Fig. 6b. Further dissection of the resistance elements needs using voltage probes to subtract the current of each electrode layer and quantify each resistance independently.[51]

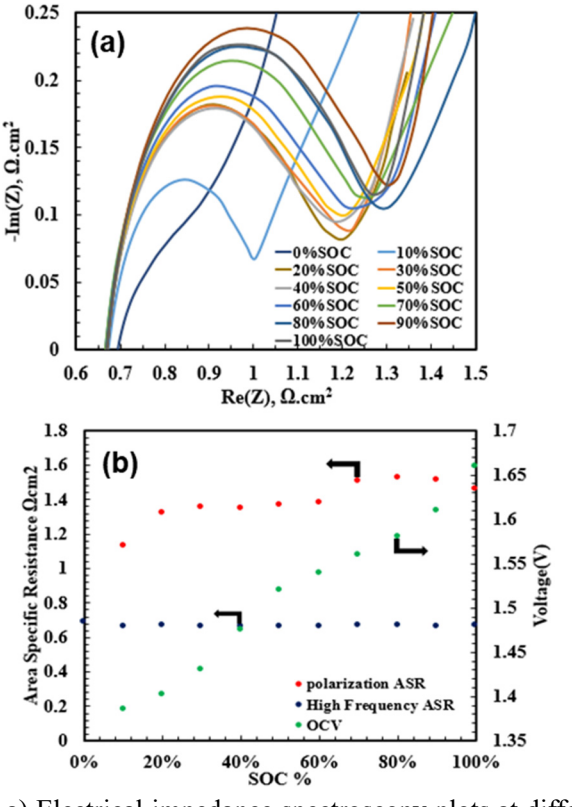

Fig. 6 a) Electrical impedance spectroscopy plots at different state of charges b) ohmic and polarization area specific resistances (ASR) as well as open circuit voltage (OCV) plotted as a function of state of charge (SOC).

© Engineered Science Publisher LLC 2020

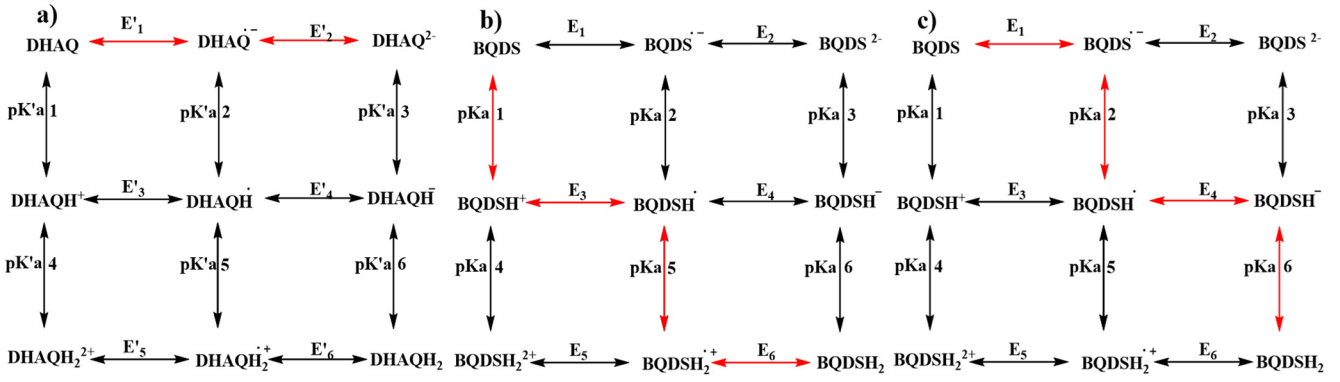

Fig. 7 Scheme of square for benzoquinone disulfonic acid (BQDS). Red arrows show the predominant reaction pathway for BQDS at acidic media. a) Assumed reaction mechanism for DHAQ b) Proposed reaction mechanism for HQDS at pH<2, c) proposed reaction mechanism for HQDS at pH>2. Change in reaction mechanism is accompanied by reduction in overall electrochemical reversibility.

Similarly, through incremental charging, open-circuit voltage of the battery is measured. For measuring an accurate OCV, sufficient time is given to the system to reach a stable potential. An OCV of 1.51 V and 1.66 V is obtained at the SOC of 50% and 100%, respectively. High OCV of the flow battery during incremental charging suggests that it is able to provide a high potential difference that enables higher voltage operations. The equilibrium cell potential and SOC equations are shown below (Eqs. (6-9)):

$$\text{Cathode:} \quad \text{BQDS}+2\text{H}^+ + 2\text{e} \rightleftharpoons \text{HQDS} \qquad E^0 = +0.85 \text{ V vs SHE} \tag{6}$$

$$\text{Anode:} \quad \text{DHAQ}+2\text{H}_2\text{O}+2\text{e} \rightleftharpoons \text{THAC}+2\text{OH}^- \qquad E^0 = -0.67 \text{ V vs SHE} \tag{7}$$

$$E_{Cell(OCV)} = \left(E^0_{Cathode} - E^0_{Anode}\right) - \left(\frac{RT}{nF}\right) \ln\left(\frac{[\text{HQDS}][\text{DHAQ}]}{[\text{BQDS}][\text{THAC}]}\right) \tag{8}$$

$$SOC(\%) = \frac{[\text{BQDS}]}{[\text{BQDS}]+[\text{HQDS}]} = \frac{[\text{THAC}]}{[\text{THAC}]+[\text{DHAQ}]} \tag{9}$$

where THAC stands for 2, 6, 9, 10 tetrahydroxy anthracene, which is the reduced form of DHAQ. The above equations also enable us to calculate the Nernstian equilibrium potential changes at different states of charge.

3.7 Analysis of Coulombic efficiency of HQDS

Quinone compounds have fast electron transfer kinetics; however, their reaction rates do not follow the same path when they are dissolved in acidic comparing to alkaline environment. Base on the mechanism called "scheme of squares" first studied by J. Jacq[50] and then referred by McAuley,[24] Wedege,[40] in alkaline media charge transfer follows two consecutive electron transfer steps while in acidic media each electron transfer reaction is accompanied by a proton transfer step which might precede or succeed the corresponding electron transfer step depending on the electrolyte pH. The scheme for bezoquinone disulfonic acid is shown in Fig. 7.

Thus, DHAQ that is dissolved in highly alkaline solution (2 M KOH) follows the first route, while HQDS dissolved in acidic media follows the second mechanism comprising of two consecutive steps, each of which contains one protonation and one electron transfer step, and their order varies depending on the electrolyte pH. Therefore, the overpotential loss and reversibility of the redox mediators are fairly different in acidic and alkaline media. All these combined factors, lead the charge transfer kinetics of the DHAQ to be larger than that of HQDS. The kinetic loss at the cathode will show itself in the potential loss in the galvanostatic graph similar to the polarization graph and can be further verified and dissected by utilization of a dynamic hydrogen electrode and running EIS.[52,53] However, the rate constants of both quinone mediators are still higher than the reactions involved in all vanadium flow batteries.[54] Both sides of the battery are excluded from air via argon gas blanketing to prevent re-oxidation of hydroquinone to quinone thus losing coulombic efficiency. DHAQ (anode) is reacting according to the following reactions during charging and discharging (Eqs. (10-11)):

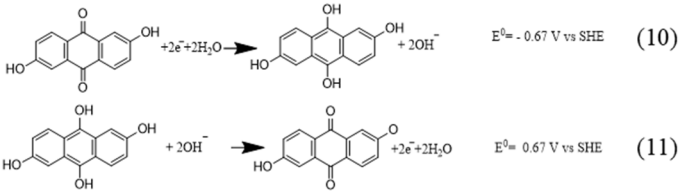

The media is alkaline and the side reactions are:

$$2\text{H}_2\text{O}+2\text{e}^- \rightleftharpoons \text{H}_2(\text{g})+2\text{OH}^- \qquad E^0 = -0.82 \text{ V vs SHE} \tag{12}$$

$$\text{O}_2(\text{g})+2\text{H}_2\text{O}+4\text{e}^- \rightleftharpoons 4\text{OH}^- \qquad E^0 = +0.40 \text{ V vs SHE} \tag{13}$$

At the anode, DHAQ may compete with hydrogen evolution reaction during charging and oxygen evolution reaction during discharging. OER is a sluggish reaction due to

 © Engineered Science Publisher LLC 2020

its 4-electron transfer process. At the time of charging, the anode potential is reduced to lower than -0.670 V vs SHE, and it is still higher than -0.827 V vs SHE for the equilibrium potential HER. Fortunately, HER is kinetically sluggish on carbon paper in alkaline media, which makes side reactions inferior to compete with the main redox reaction. Thus, there is almost no concern that DHAQ facing HER as a side reaction, and it demonstrates high coulombic efficiency, in addition to its fast kinetics. This phenomenon was also witnessed when DHAQ was coupled to ferricyanide ion in a flow battery.[44]

On the other hand, at the cathode, the redox reactions of HQDS occur according to the following reactions during charging and discharging (Eqs. (14-15)):

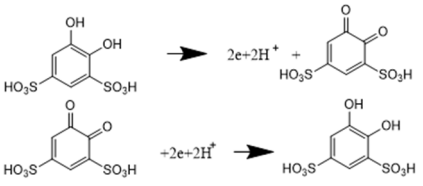

(14)

(15)

Michael Reaction (Eqs. (16)) which is the main deactivation mechanism for the cathode active material (HQDS), can lead to the irreversible battery performance loss and reduces its operation stability and cell durability, thus requiring the supply of redox mediators to the battery cathode.

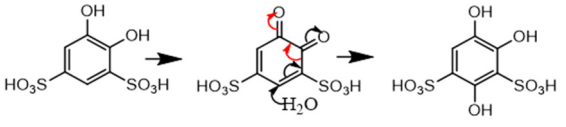

(16)

The media is acidic and the side reactions are:

$$2H^+ + 2e^- \rightleftharpoons H_2(g) \qquad E^0 = 0.00 \text{ V vs SHE} \quad (17)$$

$$O_2(g) + 4H^+ + 4e^- \rightleftharpoons 2H_2O \qquad E^0 = 1.23 \text{ V vs SHE} \quad (18)$$

Similarly, HQDS may also compete with hydrogen evolution reaction (HER) during charging and oxygen evolution reaction (OER) during discharging. However, during the charging process, the cathode voltage will be lower than – 0.85 V. Such as a low potential provides a good margin from HER potential in acidic media even though the HER reaction has to overcome the overpotential on carbon paper. Despite the fact that the kinetics of HQDS is higher than HER, in higher state of charge when less amount of HQDS ions cover the electrode surface and more protons are accessible to the electrode surface in acidic media, there is a chance for HER which lowers CE at higher SOC %.

This phenomenon is successfully prevented in this system battery by considering a higher charging rate versus the discharging rate. Exchange current density of HQDS is almost three orders of magnitude higher than the one of HER, which renders the side reaction unlikely to compete the main reaction when the battery is not fully charged (SOC<60%).

3.8 Another demonstration of this technique (DHAQ vs Fe^{+2}/Fe^{+3} flow battery)

This technique has been successfully applied to another redox consisting Fe^{2+}/Fe^{3+} coupled to 2,6 DHAQ. 1 M $FeCl_2$ and 1 M KCl are dissolved in 3 M HCl, and DHAQ is dissolved in 2 M KOH, thus having a concentrated acid at the catholyte and a concentrated base in the anolyte. Half-cell tests are reported in the literature. The reactions are as following:

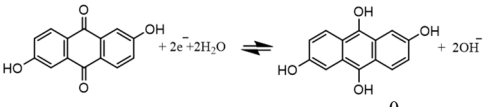

$$E^0 = -0.67 \text{ V vs SHE} \quad (19)$$

$$Fe^{3+} + e^- \rightleftharpoons Fe^{2+} \qquad E^0 = 0.77 \text{ V vs SHE} \quad (20)$$

Cell structure is similar to the previous test with argon blanketing throughout the test. Potassium ions (K^+) transport through the cation-exchange membrane (Nafion N212). The battery is charged and discharged with 100 mA/cm^2 and 60 mA/cm^2 respectively, displaying a start of discharge plateau at 1.4 V, a coulombic efficiency of 99.9% and energy efficiency of 70%. This test provides us with another example of utilizing electrolytes with contrasting pH at both sides of a single CEM, one being completely in acidic media and the other being an alkaline media, and this system can be utilized to enhance the voltage span and the energy density accordingly.

3.9 Feasibility of this technique

The proposed hybrid acid-base electrolyte flow battery has demonstrated the capability of gaining higher voltage, higher energy density, as well as stable long term pH and this system is financially advantageous over using an extra ion exchange membrane (one AEM and one CEM) to couple acid and base electrolytes in a flow battery, considering fixed costs, operation costs as well as maintenance costs.

Storage of renewable energy will necessitate the utilization of large-scale flow batteries benefiting from larger storage tanks and recirculating pumps to accommodate energy storage requirements as well as large number of cells connected in series to deliver the anticipated output power. Injection pumps have just the duty of compensating the ions that have been carried through the membranes and by using pure electrolytes (acid or base to be injected), the size of injection pumps will be considerably less than the main recirculating pumps. However, in the case that two ion-exchange membranes (one AEM and one CEM) are used to couple the acid and base electrolytes, the quantity of the membranes used will become double and by considering the fact that membranes account for almost 40% of the cost of redox flow batteries,[17,55,56] the cost impact will be considerably higher than just using two injection pumps for the whole system.

© Engineered Science Publisher LLC 2020

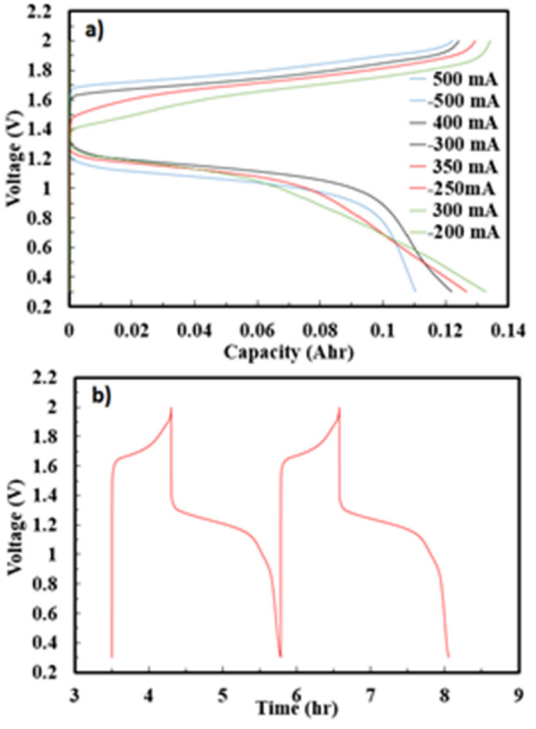

Fig. 8 a) Galvanostatic cycling of Fe/DHAQ flow battery at different charging/discharging currents, b) sample cycles of the system with charging current density of 100 mA/cm2 and discharge current density of 60 mA/cm^2.

The operation cost of this technique is also less than employing an extra membrane. Even though the ion-exchange membrane doesn't consume electricity directly, it accounts for a considerable proportion of the ohmic loss in a flow battery.[44] Thus, an extra membrane will impose further ohmic potential loss to the entire system, thus reducing the overall output voltage as well as voltage efficiency. However, the energy consumption by the injection pumps is dependent on the volume of the injected material, which will be low due to the high concentration of the added materials. Since the pumps are separated from the battery cell, they will not have any influences on voltage efficiencies.

Maintenance cost of this hybrid electrolyte flow battery is less than using extra ion-exchange membranes. Even though the life cycle of IEMs is considered to be 20 years under very optimistic estimation, ion exchange membranes, especially anion exchange membranes,[57] have low mechanical strengths and weak chemical stability in contrast to other components used in a flow battery. A small pinhole can render the membrane useless and replacement becomes necessary. Furthermore, the impact resistance of membranes are not generally sufficient and metal dendrites or mishandling can easily break them. In comparison, pumps are much more robust, although they will face abrasion or corrosion, the spare parts can be easily replaced for a long-time stable use of a pump. Moreover, the cost of replenishing the interim electrolyte in the system with two IEMs also needs to be taken into account.

Injection of chemicals is needed during the operation time of the battery and its quantity is dependent on the active surface area of the membrane. Thus, estimation of the chemical consumption requires determination of the limiting current density of the flow battery with the membrane type used. Limiting current density is a function of the mass transfer coefficient and also a function of the velocity through the battery. By using the models derived for all vanadium redox flow batteries,[58,59] it is possible to estimate the amount of chemical used per Kwh of the energy. The relevant equations and determination methods are shown below.

$$i_l = nFk_mC_b \quad (21)$$

$$k_m = 1.6*10^{-4}v^{0.4} \quad (22)$$

$$v = \frac{QL_{avg}}{A_pL_p\varepsilon} \quad (23)$$

By considering the electrode active area to be 4 cm^2, electrode porosity (ε) to be 93% after compression, assuming a tortuosity L_{avg}/L_p of 1.09 from the literature[18] and flow rate (Q) of 100 ml/min, mean electrolyte velocity will be 29.3 cm/min, yielding a mass transfer coefficient of 1.2×10^{-4} cm/s and a limiting current density of 1.27 A/cm^2 for the current through membrane. Considering operation to be at 80% of the limiting current density, storage of 1 Kwh energy in this battery will consume 85 ml of 1 M HCl and 39.6 mg of KOH with the purity of 85%. Based on the current price of HCl (35%) and KOH to be 165 $/MT (Kemcore, USA) and 350 $/MT (Qingdao Sansino, PRC) respectively, the total chemical cost with this technology will be 0.006 $/kWh. It is possible to optimize such values as well as operating conditions and even reduce the related costs.

Indeed, electrolyte acidification has been successfully utilized in the electrochemical industry specifically in large-scale chloralkali process,[60] a 5 billion dollar world market value. It is very well known that the cation exchange membrane (commonly Na^+ type Nafion membrane) is used to separate anode and cathode of a chloralkali cell, where chlorine (Cl_2) evolution reaction takes place at the anode with anolyte pH of 2-4 and alkali (NaOH) formation occurs at the cathode with catholyte pH of ~14 (0.9 M).[60] Large scale implementation of the hybrid acid-base flow battery will require the installation of online pH meters on both tanks and connecting them to the injection pump control systems. Solid base (such as KOH powder) can be directly added to the anolyte tank using a solid handling and metering system. Concentrated acid in small volume can be directly pumped into catholyte tank through an intermittent volumetric injection pump to maintain the desired low pH.

4. Conclusions

In this work, a novel flow battery with a single cation-exchange membrane and hybrid acid and base electrolytes has

 © Engineered Science Publisher LLC 2020

been successfully demonstrated with both organic quinone and inorganic iron mediators. The DHAQ - HQDS flow battery has achieved an energy density of 27.41 Wh/kg at an open circuit voltage of 1.5V with a coulombic efficiency of 99.9% at charging current density of 80 mA/cm^2 and a discharge current density of 40 mA/cm^2. Its durability has been tested for more than 140 hours and proved to be stable. In the DHAQ - Fe^{2+}/Fe^{3+} system, a concentrated acid (3 M HCl) and a concentrated base (2 M KOH) has been used at both sides of the membrane. A high coulombic efficiency of 99% with a charging current density of 100 mA/cm^2 and a discharging current density of 60 mA/cm^2 has been demonstrated.

Employing anolyte and catholyte with contrasting pH may open a new avenue to operating battery with broader voltage range and to couple various kinds of redox mediators, thus enabling the rational design of new batteries with higher operation voltage, charging/discharging power density and energy density. This technology can be specifically useful for those redox mediators that highly rely on deprotonation during their redox reactions, therefore enhancing the voltage span as well as the energy density harnessed from the flow battery.

Hydroquinone disulfonic acid (HQDS) has been chosen for concept proof because it has the highest redox potential of all quinone compounds (0.86 V vs. SHE) and also owns a very high solubility of 1.7 M in aqueous systems[42] and is also able to be used at pH=7, however more of its redox span is used if it is utilized in acidic media. In this configuration, HOMO of DHAQ is lowered by the presence of 2 hydroxyl groups, while LUMO of HQDS is raised by the presence of two sulfonic acid groups, finally raising the cell potential.[61]

There is plenty of room to design more efficient quinone molecules, for example, filling the empty locations in HQDS with more electron withdrawing groups can not only increase the redox potential even further but also alleviate the deactivation issue mainly caused by the Michael mechanism.[33] Simultaneously, higher solubility and diffusion coefficient of HQDS will result in a smaller Nernst diffusion layer and a more effective mass transport coefficient. Possibility of side reactions (HER) can be reduced by operating at a lower state of charge (SOC) as well as modification of electrode materials that can increase HER overpotential even further. All these attributes make HQDS a promising candidate to be used as cathode material in redox flow batteries and also provide future opportunities to work on its structure and augment its characteristics.

Online monitoring of the SOC of this system via UV-vis similar to the case that has been used for all vanadium flow batteries[62] is not applicable here due to the very high absorbance of the components specifically the anode material. However, the effect of electrode material, structure and its degradation on suppressing side reactions (e.g. hydrogen evolution reaction), which reduce the energy efficiency can be considered by measuring the *in situ* charge transfer kinetics via electrical impedance spectroscopy and constructing the Tafel plots,[63] analyzing ECSA effect,[53] benefiting from series technique,[64] utilization of a printed board circuit between flow channel plate and current collector[65] or placing potential probes between electrodes and connecting them to a dynamic hydrogen electrode.[66,67]

Acknowledgments

This research was partly funded by Iowa State University Bailey Career Development Award. W. Li acknowledges his Richard Seagrave Professorship and Ames Lab startup fund. M. Torabi is grateful to the Exploratory Research Program (ERP) fund from College of Engineering, Iowa State University.

Conflict of Interest

There is no conflict of interest.

Supporting Information

Not Applicable.

References

[1] P. Ravestein, G. Schrier, R. Haarsma, R. Scheele and M. Broek, *Renew. Sust. Energ. Rev.*, 2018, **97**, 497-508, doi: 10.1016/j.rser.2018.08.057.

[2] G. Notton, M. Nivet, C. Voyant, C. Paoli, C. Darras, F. Motte and A. Fouilloy, *Renew. Sust. Energ. Rev.*, 2018, **87**, 96-105, doi: 10.1016/j.rser.2018.02.007.

[3] A. Brouwer, M. Broek, A. Seebregts and A. Faaij, *Renew. Sust. Energ. Rev.*, 2014,**33**, 443-466, doi: 10.1016/j.rser.2014.01.076.

[4] M. Melikoglu, *Renew. Sust. Energ. Rev.*, 2017, **72**, 146-153, doi: 10.1016/j.rser.2017.01.060.

[5] S. Zhou, J. Zhang, W. Song and Z. Feng, *Energy Procedia*, 2018, **152**, 162-167, doi: 10.1016/j.egypro.2018.09.075.

[6] F. P. Sioshansi, *Distributed Generation and its Implications for the Utility Industry*, 2014, xxxiii-li, doi: 10.1016/B978-0-12-800240-7.09988-4.

[7] G. L. Soloveichik, *Chem. Rev.*, 2015, **115**, 11533-11558, doi: 10.1021/cr500720t.

[8] B. Dunn, H. Kamath and J.M. Tarascon, *Science*, 2011, **334**, 928-935, doi: 10.1126/science.1212741.

[9] Y. Yang, S. Bremner, C. Menictas and M. Kay, *Renew. Sust. Energ. Rev.*, 2018, **91**, 109-125, doi: 10.1016/j.rser.2018.03.047.

[10] Y. Zeng, J. Hu, W. Ye, W. Zhao, G. Zhou and Y. Guo, *J. Power Sources*, 2015, **286**, 182-192, doi: 10.1016/j.jpowsour.2015.03.139.

[11] P. Hundekar, S. Basu, J. Pan and N. Koratkar, *Energy Storage Materials*, 2019, **20**, 291-298, doi: 10.1016/j.ensm.2019.04.013.

[12] C. Zhang, J. Xu, L. Cao, Z. Wu and S. Santhanagopalan, *J. Power Sources*, 2017,**357**, 126-13710.1016/j.jpowsour.2017.04.103.

[13] C. Chen, Y. Wei, Z. Zhao, Y. Zou and D. Luo, *Electrochim. Acta*, 2019, **305**, 65-71, doi: 10.1016/j.electacta.2019.03.038.

[14] M. L. Perry and A.Z. Weber, *J. Electrochem. Soc.*, 2016, **163**, A5064-A506710.1149/2.0101601jes.

© Engineered Science Publisher LLC 2020

[15] M. Zhang, M. Moore, J.S. Watson, T.A. Zawodzinski and R.M. Counce, *J. Electrochem. Soc.*, 2012, **159**, A1183-A1188, doi: 10.1149/2.041208jes.
[16] C. Bae, E. Roberts and R. Dryfe, *Electrochim. Acta*, 2002, **48**, 279-287, doi: 10.1016/S0013-4686(02)00649-7.
[17] Y. K. Zeng, T.S. Zhao, L. An, X.L. Zhou and L. Wei, *J. Power Sources*, 2015, **300**, 438-443, doi: 10.1016/j.jpowsour.2015.09.100.
[18] M. Matyka, A. Khalili and Z. Koza, *Phys. Rev. E*, 2008,**78**, 026306, doi: 10.1103/PhysRevE.78.026306.
[19] M. Vijayakumar, W. Wang, Z. Nie, V. Sprenkle and J. Hu, *J. Power Sources*, 2013, **241**, 173-177, doi: 10.1016/j.jpowsour.2013.04.072.
[20] S. Rudolph, I. Bayanov, G. Pfeiffer and U. Schröder, *J. Electroanal. Chem.*, 2013, **709**, 93-98, doi: 10.1016/j.jelechem.2013.09.033.
[21] H. Liu, Q.Xu, C.Yan and Y. Qiao, *Electrochim. Acta*, 2011, **56**, 8783-8790, doi: 10.1016/j.electacta.2011.07.083.
[22] S. Bae, J. Lee and D.S. Kim, *J. Power Sources*, 2019, **413**, 167-173, doi: 10.1016/j.jpowsour.2018.12.038.
[23] D. Bryans, B.G. McMillan, M. Spicer, A. Wark and L. Berlouis, *J. Electrochem. Soc.*, 2017, **164**, A3342-A3348, doi: 10.1149/2.1651713jes.
[24] C. Batchelor-McAuley, Q. Li, S.M. Dapin and R.G. Compton, *J. Phys. Chem. B*, 2010,**114**, 4094-4100, doi: 10.1021/jp1008187.
[25] P. Leung, A. Shah, L. Sanz, C. Flox, J.R. Morante, Q. Xu, M. Mohamed, C. León and F. Walsh, *J. Power Sources*, 2017,**360**, 243-283, doi: 10.1016/j.jpowsour.2017.05.057.
[26] J. Winsberg, T. Hagemann, T. Janoschka, M.D. Hager and U.S. Schubert, *Angew. Chem. Int. Edit.*, 2017,**56**, 686-711, doi: 10.1002/anie.201604925.
[27] R. M. Darling, K.G. Gallagher, J.A. Kowalski, S. Ha and F.R. Brushett, *Energ. Environ. Sci.*, 2014, **7**, 3459-3477, doi: 10.1039/c4ee02158d.
[28] H. Chen, G. Cong and Y.C. Lu, *J. Energ. Chem.*, 2018,**27**, 1304-1325, doi: 10.1016/j.jechem.2018.02.009.
[29] T. Liu, X. Wei, Z. Nie, V. Sprenkle and W. Wang, *Adv. Energy Mater.*, 2016, **6**, 1501449, doi: 10.1002/aenm.201501449.
[30] E. S. Beh, D. De Porcellinis, R.L. Gracia, K.T. Xia, R.G. Gordon and M.J. Aziz, *ACS Energy Lett.*, 2017, **2**, 639-644, doi: 10.1021/acsenergylett.7b00019.
[31] B. Hu, C. DeBruler, Z. Rhodes and T.L. Liu, *J. Am. Chem. Soc.*, 2017, **139**, 1207-1214, doi: 10.102l/jacs.6b10984.
[32] B. Huskinson, M.P. Marshak, C. Suh, S. Er, M.R. Gerhardt, C.J. Galvin, X. Chen, A. Aspuru-Guzik, R.G. Gordon and M.J. Aziz, *Nature*, 2014, **505**, 195-198, doi: 10.1038/nature12909.
[33] L. Hoober-Burkhardt, S. Krishnamoorthy, B. Yang, A. Murali, A. Nirmalchandar, G.K.S. Prakash and S.R. Narayanan, *J. Electrochem. Soc.*, 2017, **164**, A600-A607, doi: 10.1149/2.0351704jes.
[34] S. Er, C. Suh, M.P. Marshak and A. Aspuru-Guzik, *Chem. Sci.*, 2015,**6**, 885-893, doi: 10.1039/c4sc03030c.
[35] M. R. Gerhardt, L. Tong, R. Gómez-Bombarelli, Q. Chen, M.P. Marshak, C.J. Galvin, A. Aspuru-Guzik, R.G. Gordon and M.J. Aziz, *Adv. Energy Mater.*, 2017,**7**, 1601488, doi: 10.1002/aenm.201601488.
[36] Z. Yang, L. Tong, D.P. Tabor, E.S. Beh, M.A. Goulet, D. De Porcellinis, A. Aspuru-Guzik, R.G. Gordon and M.J. Aziz, *Adv. Energy Mater.*, 2018, **8**, 1702056, doi: 10.1002/aenm.201702056.
[37] Q. Chen, M.R. Gerhardt, L. Hartle and M.J. Aziz, *J. Electrochem. Soc.*, 2016, **163**, A5010-A5013, doi: 10.1149/2.0021601jes.
[38] D. G. Kwabi, K. Lin, Y. Ji, E.F. Kerr, M.A. Goulet, D.D. Porcellinis, D.P. Tabor, D.A. Pollack, A. Aspuru-Guzik, R. Gordon and M.J. Aziz, *Joule*, 2018, **2**, 1894-1906, doi: 10.1016/j.joule.2018.07.005.
[39] Y. Ji, M.A. Goulet, D.A. Pollack, D.G. Kwabi, S. Jin, D. De Porcellinis, E.F. Kerr, R.G. Gordon and M.J. Aziz, *Adv. Energy Mater.*, 2019,**9**, 1900039, doi: 10.1002/aenm.201900039.
[40] K. Wedege, E. Dražević, D. Konya and A. Bentien, *Sci. Rep-UK*, 2016,**6**, 39101, doi: 10.1038/srep39101.
[41] S. Gu, K. Gong, E.Z. Yan and Y. Yan, *Energ. Environ. Sci.*, 2014, **7**, 2986-2998, doi: 10.1039/c4ee00165f.
[42] B. Yang, L. Hoober-Burkhardt, F. Wang, G.K. Surya Prakash and S.R. Narayanan, *J. Electrochem. Soc.*, 2014, **161**, A1371-A1380, doi: 10.1149/2.1001409jes.
[43] J. Luo, A. Sam, B. Hu, C. DeBruler, X. Wei, W. Wang and T.L. Liu, *Nano Energy*, 2017, **42**, 215-221, doi: 10.1016/j.nanoen.2017.10.057.
[44] K. Lin, Q. Chen, M.R. Gerhardt, L. Tong, S.B. Kim, L. Eisenach, A.W. Valle, D. Hardee, R.G. Gordon, M.J. Aziz and M.P. Marshak, *Science*, 2015, **349**, 1529-1532, doi: 10.1126/science.aab3033.
[45] M.A. Goulet, L. Tong, D.A. Pollack, D.P. Tabor, S.A. Odom, A. Aspuru-Guzik, E.E. Kwan, R.G. Gordon and M.J. Aziz, *J. Am. Chem. Soc.*, 2020, **141**, 8014-8019, doi: 10.1021/jacs.8b13295.
[46] Y. Qiao, K. Jiang, X. Li, H. Deng, Y. He, Z. Chang, S. Wu, S. Guo and H. Zhou, *Adv. Energy Mater.*, 2018, **8**, 1801120, doi: 10.1002/aenm.201801120.
[47] Y. Qiao, Y. He, K. Jiang, Y. Liu, X. Li, M. Jia, S. Guo and H. Zhou, *Adv. Energy Mater.*, 2018, **8**, 1802322, doi: 10.1002/aenm.201802322.
[48] Q. H. Liu, G. M. Grim, A. B. Papandrew, A. Turhan, T.A. Zawodzinski and M.M. Mench, *J. Electrochem. Soc.*, 2012, **159**, A1246-A1252, doi: 10.1149/2.051208jes.
[49] X. Ke, J. M. Prahl, J.I.D. Alexander, J.S. Wainright, T.A. Zawodzinski and R.F. Savinell, *Chem. Soc. Rev.*, 2018, **47**, 8721-8743, doi: 10.1039/c8cs00072g.
[50] J. Jacq, *J. Electroanal. Chem.*, 1971, **29**, 149-180, doi: 10.1016/S0022-0728(71)80080-3.
[51] Q. Chen, M.R. Gerhardt and M.J. Aziz, *J. Electrochem. Soc.*, 2017,**164**, A1126-A1132, doi: 10.1149/2.0721706jes.

 © Engineered Science Publisher LLC 2020

[52] C. Sun, F. Delnick, D. Aaron, A. Papandrew, M. Mench and T. Zawodzinski, *ECS Electrochem. Lett.*, 2013, **2**, A43-A45, doi: 10.1149/2.001305eel.
[53] D. Aaron, C.N. Sun, M. Bright, A.B. Papandrew, M.M. Mench and T.A. Zawodzinski, *ECS Electrochem. Lett.*, 2013, **2**, A29-A31, doi: 10.1149/2.001303eel.
[54] J. M. Hale and R. Parsons, *Transactions of the Faraday Society*, 1963, **59**, 1429-1437, doi: 10.1039/tf9635901429.
[55] H. Kamath and S. Rajagopalan, Vanadium Redox Flow Batteries: An In-Depth Analysis (Technical Report), EPRI, Palo Alto, CA (2007).
[56] P. Leung, T. Martin, M. Anderson, J. Palma, A. Shah and M. Mohamed, *J. Power Sources*, 2017, **341**, 36-45, doi: 10.1016/j.jpowsour.2016.11.062.
[57] S. Gottesfeld, A. Dekel, M. Page, C. Bae, Y. Yan, P. Zelenay and Y.S. Kim, *J. Power Sources*, **375**, 2018, 170-184, doi: 10.1016/j.jpowsour.2017.08.010.
[58] Y. Dongjie, H. Zhang and J. Chen, *Electrochim. Acta*, 2009, **54**, 6827-6836, doi: 10.1016/j.electacta.2009.06.086.
[59] J.Y. Chen, C.L. Hsieh, N.Y. Hsu, Y.S. Chou and Y.S. Chen, *Energies*, 2014,**7**, 5863-5873, doi: 10.3390/en7095863.
[60] R. K. Karlsson and A. Cornell, *Chem. Rev.*, 2016, **116**, 2982-3028, doi: 10.1021/acs.chemrev.5b00389.
[61] W. T. Simpson, *J. Chem. Educ.*, 1962,**39**, 434, doi: 10.1021/ed039p434.2.
[62] Z. Tang, D.S. Aaron, A.B. Papandrew and T.A. Zawodzinski, *ECS Transactions*, 2012, **41**, 1-9, doi: 10.1149/1.3697449.
[63] C.N. Sun, F.M. Delnick, D.S. Aaron, A.B. Papandrew, M.M. Mench and T.A. Zawodzinski, *J. Electrochem. Soc.*, 2014, **161** , A981-A988, doi: 10.1149/2.045406jes.
[64] A. M. Pezeshki, R.L. Sacci, G.M. Veith, T.A. Zawodzinski and M.M. Mench, *J. Electrochem. Soc.*, 2016, **163**, A5202-A5210, doi: 10.1149/2.0251601jes.
[65] J. T. Clement, T.A. Zawodzinski, M.M. Mench, *ECS Transactions*, 2013, **58**, 9-16, doi: 10.1149/05837.0009ecst.
[66] D. S. Aaron, Z. Tang, J.S. Lawton, A.P. Papandrew and T.A. Zawodzinski, *ECS Transactions*, 2012,**41**, 43-51, doi: 10.1149/1.3697453.
[67] Q. Liu, A. Turhan, T.A. Zawodzinski and M.M. Mench, *Chem. Commun.*, 2013, **49**, 6292-6294, doi: 10.1039/c3cc42092b.

Publisher's Note

Engineered Science Publisher remains neutral with regard to jurisdictional claims in published maps and institutional affiliations.

© Engineered Science Publisher LLC 2020